Use of Footprint Maps to Support Positioning and Guidance in Visible Light Communication Technology

Paula Louro, Manuela Vieira, Manuel Augusto Vieira
DEETC/ISEL/IPL,
R. Conselheiro Emídio Navarro, 1959-007
Lisboa, Portugal

CTS-UNINOVA
Quinta da Torre, Monte da Caparica, 2829-516,
Caparica, Portugal
e-mail: plouro@deetc.isel.pt, mv@isel.ipl.pt,
mvieira@deetc.isel.pt

***Abstract*— Due to the general, worldwide need for communication, Visible Light Communication (VLC) has become a research topic today. In comparison to other wireless technologies (such as Wi-Fi), this technology combines lighting and communication, enabling high data rates and reliability. In this paper VLC is used to establish different optical communication links for bidirectional communication between infrastructures and vehicles, namely Infrastructure-To-Vehicle (I2V) and Vehicle-To-Infrastructure (V2I). VLC is used to provide guidance and management services for autonomous robot navigation inside an automated warehouse. Specific coding schemes are used in each optical link. The I2V link uses RGB white LEDs to simultaneously modulate the emitters embedded in each LED, allowing wavelength division multiplexing of optical signals transmitted via this link. The detection is based on an a-SiC:H pin-pin photodetector with tunable sensitivity in the visible range. The impact of parity check bits on bit error rate is discussed for different indoor communication scenarios.**

Keywords- Visible Light Communication; Indoor guidance; White LEDs; Lambertian model; navigation cell.

I. INTRODUCTION

This paper is an extension of work originally presented in ALLSENSORS 2022 [1] that provided preliminary results of the use of footprint maps to support positioning and guidance under visible light communication technology. This work discusses the use of the footprint maps for this purpose and the importance of proper decoding methods.

Indoor positioning can be addressed by several techniques, such as Wi-Fi, Assisted GPS (A-GPS), Infrared, Radio Frequency Identification (RFID), and many other technologies [2][3]. Visible Light communication (VLC) is also an alternative, enhanced accuracy technology. VLC operates with visible light extending from 400 nm up to 750 nm [4][5]. VLC systems use modulated LEDs to transmit information [6]. Due to its characteristics, LEDs [7] can be switched very fast to produce modulated light in high frequencies, allowing data transmission in high speed. For lighting purposes, energy saving demands the use of white LEDs [8][9], either based on blue emitter coated with a phosphor layer or based on polychromatic emitters. Phosphor-based LEDs usually consist of a blue LED chip covered in a yellow phosphor layer. Due to the long relaxation time of the phosphor, when this LED is used for VLC, the modulation bandwidth is limited, thereby limiting the transmission capacity. Using a blue filter before the receiver unit can increase the LED modulation bandwidth by eliminating the slow response of the yellow light component [10][11]. Although tri-chromatic LEDs are more expensive, they provide more bandwidth due to the independent modulation of each chip of a monolithic device.

The receiver unit of VLC systems usually includes silicon-based photodiodes, as these devices operate in the visible region of the spectrum, or CMOS image sensors [12][13].

In this paper we propose the use of a multilayered a-SiC**:**H [14] [15] device to perform the photodetection of the optical signals generated by white trichromatic RGB LEDs [16], [17]. The system was designed for positioning and guidance [18][19], and the transmitters of each white LED were specifically modulated at precise frequencies and coding bit sequences [20][21].

The optical VLC channel is characterized through the prediction of the channel gain, taking into consideration emitter characteristics, optical channel features and receiver properties. The Lambertian model is used for LED light distribution and MatLab simulations are used to infer the signal coverage of the LED in the illuminated indoor space [22][23]. The decoding strategy of the multiplexed signals demands system calibration for accurate regulation of each photocurrent level [24][25] and preferably the use of bit error control strategies, which are also discussed. For each link, different codification schemes are proposed using On-Off keying modulation.

The proposed lighting and positioning/guidance system involves wireless communication, computer-based algorithms, smart sensor, and optical sources network, which constitutes a transdisciplinary approach framed in cyber-physical systems.

The paper is organized as follows. After the introduction (Section I), the general description of the system is presented in Section II. In Section III, the communication protocol and the encoding/decoding techniques are analyzed and discussed. At last, conclusions are addressed in Section IV.

II. VLC SYSTEM GENERAL DESCRIPTION

The VLC system is composed by the transmitter and the receiver modules, located at the infra-structure and at the mobile vehicle. Two optical links are established between the lamps and the vehicles, for I2V and V2I transmission. The optical source of the transmitter at infrastructure consists of four white RGB LEDs, while at a vehicle it is a multicolor LED or a single-color LED placed at the top. The sensor device used for the detection of the optical signals is a monolithic heterojunction composed of two pin structures [26]. As a result of its narrow thickness (200 nm) and higher bandgap (2.1 eV), the front pin a-SiC:H photodiode is responsible for the device's sensitivity to short wavelengths of the visible range (400 - 550 nm). The back pin a-Si:H structure operates in the complementary past of the visible range, collecting the long wavelengths (520 nm - 700 nm) [27]. The illumination window is established on the front photodiode. The use of steady state light as background light provides an enhancement of the electrical field of the front pin photodiode and the amplification of the generated photocurrent signal due to long wavelength light.

A. Transmitter configuration

For every channel of the I2V and V2I links, synchronous transmission based on a 64 bits data frame was used. In Figure 1 a) it is displayed the configuration of the LED lamp with four RGB white LEDs used in the I2V link. A uniform white light is provided in the indoor area by all three emitters (red, green, and blue). However, only specific emitters are modulated at a frequency imperceptible to the human eye. Each of these lamps illuminates an area with full radial coverage as shown Figure 1 b).

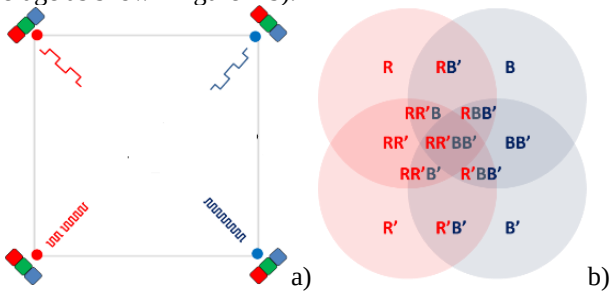

Figure 1. Configuration of the VLC emitter: a) 4 RGB white LEDs; b) coverage area of each modulated emitter.

The illuminated area corresponds to the coverage area of each lamp, defining a unit cell for the vehicle navigation along the space. The modulated emitters are the red junctions of the LEDs placed at the left side and the blue junctions of the LEDs at the right side.

For the proposed system, the commercial white LEDs were designed for illumination purposes, exhibiting a wide half intensity angle ($\phi_{1/2}$) of 120º. Thus, the Lambertian order *m* is 1. The coverage range and radiation pattern of the LED light is affected by the half intensity angle, such that narrower $\phi_{1/2}$ increases the illumination range. In Figure 2 it is displayed the luminous intensity of the red, green, and blue optical emitters of the white RGB commercial LEDs used in this system.

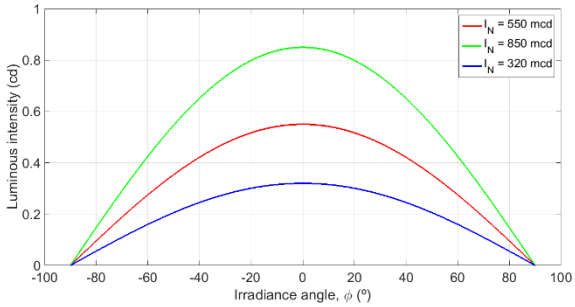

Figure 2. Distribution of luminous intensity for the red, green, and blue emitters.

For the maximum luminous intensity in the axial direction (I_N) it was considered the average values stated in the datasheet specifications [28]. As it is shown in Figure 2, the luminous intensity varies with the direction, presenting a maximum at the axial direction (0º) and half of the maximum at $\phi_{1/2}$= ± 60º.

In Figure 3 it is plotted the normalized output spectra of the RGB white LEDs driven with a biasing current of 3 mA.

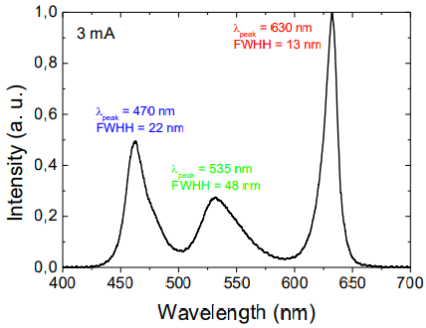

Figure 3. Output normalized spectrum of the RGB white LED.

The output spectra cover the wavelengths assigned to the blue, green and red regions, with wavelengths centered, respectively at 470 nm, 535 nm and 630 nm. The full width half height of each peak (FWHH) is 22 nm for the blue chip, nearly 48 nm for the green and 13 nm for the red chip. Usually, the FWHH of LED devices increases with the wavelength. However, as this is a white LED, the magnitude and width of each RGB peaks are optimized for the white. The green component is the lowest because the human eye has a maximum sensitivity at 530 nm.

Table I summarizes the main optical characteristics of the optical sources of the VLC transmitter.

TABLE I. OPTICAL CHARACTERISTICS OF THE WHITE LEDS AT 25 ºC.

Central wavelength (nm)	620	530	470
Luninous intensity (mcd)	628	980	340
Linewidth @ 20 mA	24	38	28
Half intensity angle (°)	± 60	± 60	± 60

B. Channel characterization

LEDs are modeled as Lambertian sources with uniform distribution of luminance in all directions, and luminous intensity dependent on the direction. The luminous intensity for a Lambertian source is given by the following equation [29]:

$$I(\phi) = I_N \cos^m(\phi) \quad (1)$$

where m is the order derived from a Lambertian pattern, I_N is the maximum luminous intensity in the axial direction and ϕ is the angle of irradiance. The Lambertian order m is given by:

$$m = -\frac{\ln(2)}{\ln(\cos(\phi_{1/2}))} \quad (2)$$

The Lambertian order m indicates the LED's half-power angle. The semi-angle represents the area illuminated by the LED radiation pattern. Generally, a small m (around 1) indicates a wide illumination region, whereas a high m relates to a highly focused illumination region. Thus, m is a measure of light source spatial directivity. In this case, as the half intensity angle ($\phi_{1/2}$) is of 60º, the Lambertian order m is 1.

The light signal is received by the photodetector, generates a binary sequence of the received signals and converts data into the original format. It is assumed Line of Sight (LoS) conditions, which consider that the signal propagation occurs in a direct path from the source to the receiver.

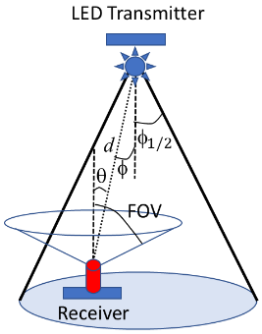

Figure 4. Transmitter and receiver relative position.

Figure 4 shows the relative position of the transmitter and receiver units with specification of the geometrical parameters needed to infer the signal coverage of the LED in the illuminated indoor space [30].

The channel gain (G) of the VLC link is given by equation [31]:

$$G = \frac{(m+1)A}{2\pi d^2} I_N \cos^m(\emptyset)\cos(\theta) \quad (3)$$

where A is the area of the photodetector, d is the distance between the emitter and the receiver, and FOV is the field of view of the detector (angular extension for signal detection).

In Figure 5 it is displayed the predicted received power of the emitters of the white RGB LED transmitter.

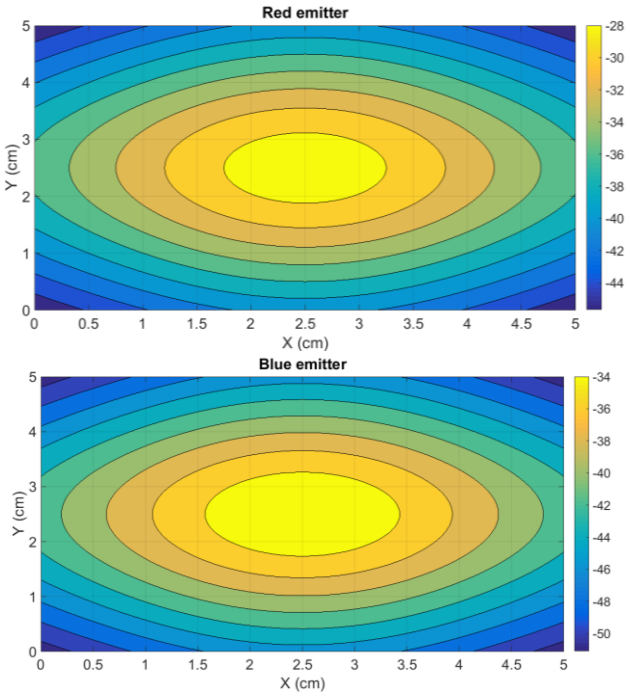

Figure 5. Received power (dBm) the red and blue emitters of the white RGB LED transmitter.

C. Footprint maps

Figure 6 illustrates the coverage map produced when only the red and blue emitters of each LED are used for data transmission. This region allows the definition of the unit navigation cell related to each luminaire of the illuminated space.

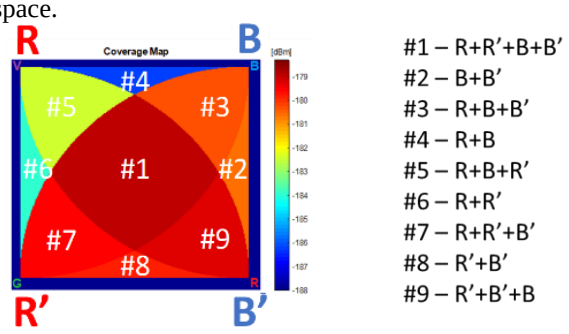

Figure 6. Coverage map of the fine-grain footprint inside the navigation cell, considering as VLC optical sources the top red and bottom blue emitters.

In each unit navigation cell, any receiver will be able to identify the emission lamp and make a correspondence to the spatial position inside the warehouse. By modulating the red and blue emitters of each lamp, the optical pattern created within each navigation cell can enhance position accuracy. Inside the navigation cell, top emitters (labelled R and B) point north, bottom emitters (R' and B') point south and left (R and R') and right (B and B') emitters point west and east, respectively.

Based on this assumption, the RB' optical pattern corresponds to the north direction, R'B' to the south, RR' to the west and BB' to the east. The intercardinal directions inside the navigation cell correspond to RR'B (northwest), RBB' (northeast), RR'B' (southwest) and R'BB' (southeast). In this coverage map the optical signal produced by each modulated LED confers a maximum of delivered power signal at the central region of the cell, that receives contribution from four modulated channels. The regions at the corners contain optical signals from three LEDs, exhibiting a decrease on the received power signal, while the side regions correspond to the lowest values of received power. Each of these regions constitute footprints of the delivered power. Each footprint region labelled as #1, #2, …, #9 is assigned to the correspondent optical excitation illustrated on the right side of Figure 6. Using adjacent LED lamps to light the indoor space, different navigation cells are enabled by each lamp. The identification of each lamp is provided by a specific code.

D. Coding

In Figure 7 it is displayed the data frame structure the bi-directional communication I2V and V2I.

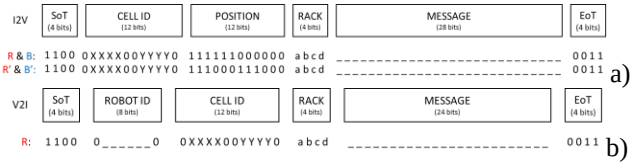

Figure 7. Data frame structure the communication: a) I2V and b) V2I channels.

Data frames are words of 64 bits composed each of six blocks. First and last blocks, labelled respectively as SoT (Start of Text) and EoT (End of Text) are used to trigger synchronization of the transmitter and receptor in each link. In the I2V link, there are also the blocks CELL ID, POSITION, RACK and MESSAGE. Identification of the unit cell is given by the block CELL ID. The format of the word code is 0XXXX00YYYY0, where XXXX addresses the line and YYYY the column of the unit navigation cell. Block POSITION provides information about which emitters are being detected by the mobile vehicle and thereby enables the vehicle to know its relative position within the navigation cell. The block RACK contains information about the stock stored inside the rack, addressing different sections. The MESSAGE block (32 bits) enables the possibility of transmitting a random message to the vehicle.

In the V2I link a single LED is used to transmit information from the vehicle to the infrastructure, namely information about items being removed from the rack within the navigation cell to the shipping station. The code word contains the blocks ROBOT ID, CELL ID, RACK and MESSAGE, besides SoT and EoT blocks. The blocks ROBOT ID and CELL ID encode the identification of the transmitting vehicle and of the receiver infrastructure. The RACK block identifies the specific rack from where items are being removed and the MESSAGE block encodes the item and quantity being removed.

E. Receiver configuration

The VLC receiver device of the system is a photodiode able to measure both pulsed and steady light sources, by converting the optical power to an electrical current, which depends on incident light power and wavelength. The photodiode is a dual sandwich pin photodetector with an a-Si:H pin structure mounted above an a-SiC:H pin structure, allowing the device to be used over the full a-Si:H and a-SiC:H wavelength ranges (Figure 8).

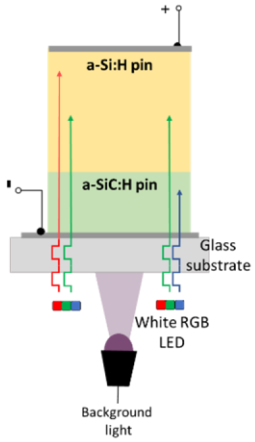

Figure 8. VLC sensor device: based on two stacked pin photodiodes based on a-SiC:H and a-Si:H.

It operates in the full range of the visible spectrum, with a spectral sensitivity that can be controlled externally using steady state light [32]. The device is housed on a glass substrate with one anode and one cathode connections. It is operated under reverse bias to improve collection efficiency. It is a large area device with a sensitive area of 1 cm^2 which contributes to the collection efficiency of light, and at the same time induces capacitive effects prone to limit speed operation.

The intrinsic layer materials used in each pin photodiode of the device and the thickness of each absorption layer provide different absorption mechanisms due to the specific material bandgaps. The used configuration delivers high absorption of short wavelength light in the front photodiode (a-SiC:H) and high absorption of the long wavelengths in the back photodiode (a-Si:H). Intermediate wavelengths are absorbed by both photodiodes. The use of steady state light as background light enhances the electrical field of the front a-SiC:H photodiode and amplifies the generated photocurrent signal produced under long wavelength light incidence.

III. RESULTS AND DISCUSSION

In the V2I link a single emitter is used to transmit information from the mobile robot to the LED infrastructure. In Figure 9 it is displayed the output signal due to the optical signal transmitted by the mobile robot after removing items

from a specific rack. On the top it is displayed the optical signal with the transmitted bit sequence. As this V2I link uses a single emitter, the photocurrent signal, when under line-of-sight condition, follows the pattern of the single transmitted optical signal. Thus, decoding is a simple process, limited only by the photodiode sensitivity at low illumination conditions.

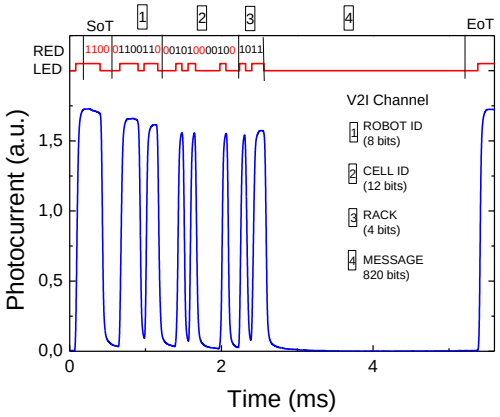

Figure 9. Output signal transmitted by the robot to the infrastructure after removal of items from the rack. On the top it displayed the transmitted optical signal.

As shown in the figure, bits in red color, either set to 1 or to 0, cannot be changed in this channel. Bits in black color are those that define the specific communication conditions. In this case, the blocks of the coded 64-bits word can be easily decoded. Bits of the ROBOT ID are 01100110, corresponding to the identification code 118 (decimal representation). The CELL ID provides for the decoded bits, the number 001010000100, which corresponds to line 5 and column 2. Bits of the RACK block are 1011, representing that items from the first and third racks were removed when the vehicle moved in the forward lane.

In the I2V link, the use of four emitters to transmit the coded information generates 16 photocurrents levels, assigned to 16 different optical excitations. These levels are dependent on the optical intensity at the reception end, however, its relative position is assumed to be constant. This supports the use of a calibration curve to demultiplex the signal, decodes the transmitted bits and enables identification of the input optical signals. In Figure 10 it is displayed the calibration curve, showing the 16 output levels assigned to each input optical state. The driving current of each LED emitter was adjusted to provide different levels of photo excitation.

On the right side of the picture, it is shown the label of the modulated emitters that correspond to each photocurrent level. The decoding methodology based on the calibration curve may result in some error mismatch when the photocurrent levels are too close. It is important to mention that only 9 of these 16 levels are used to infer the position using the footprint maps. Thus, the correct decoding of these levels is crucial to support positioning.

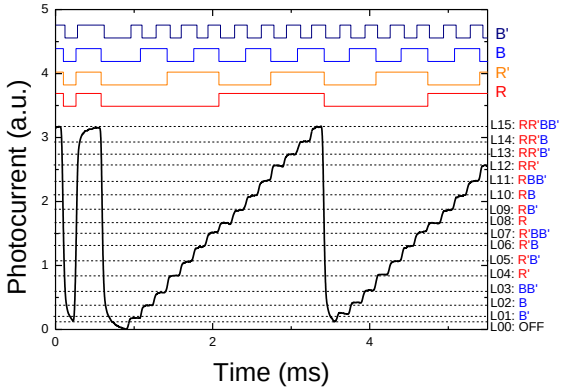

Figure 10. Calibration photocurrent signal using two red and two blue optical signals (on the top it is displayed the waveform of the emitters modulation state).

To increase the accuracy of the decoding task, bit error detection with parity check bits can be used. Parity bits (P1, P2, P3) assigned to the 4 transmission channels (R, R', B, B') are evaluated using a simple algorithm that sums up the bits transmitted by 3 of the channels:

$$P1 = R + R' + B'$$
$$P2 = R' + B + B' \quad (4)$$
$$P3 = R + B + B'$$

In Figure 11 it is displayed the parity check bits evaluated by equation (1) for the transmission of the bit sequences plotted in Figure 10. The parity check bits sequences (P1, P2 and P3) are transmitted, respectively, by the R, R' and B emitters.

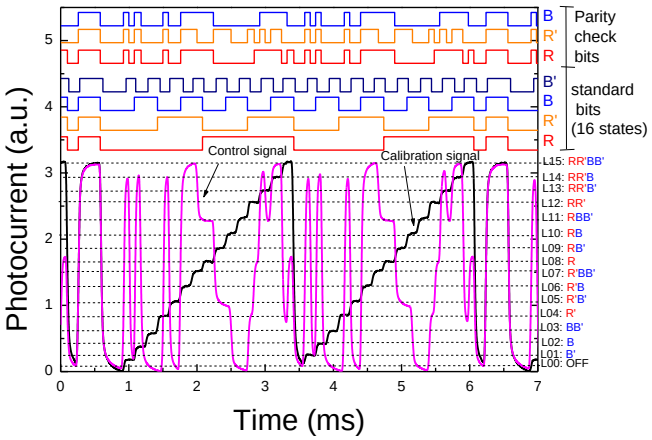

Figure 11. Calibration data and correspondent error control signal obtained by the transmission of the parity check bits.

Results show that the error control signal can be used to help on the decode process when photocurrent levels are very close. Under these circumstances, the use of parity check bits can detect and correct errors without the need to discard the transmitted data from the specific error bit and re-transmit it again.

In Figure 12 it is displayed the photocurrent signal acquired along the forward lane at positions under the coverage of RR'BB'. In superposition it is displayed the calibration grid. At the top it is displayed the input optical signals (R, R', B and B').

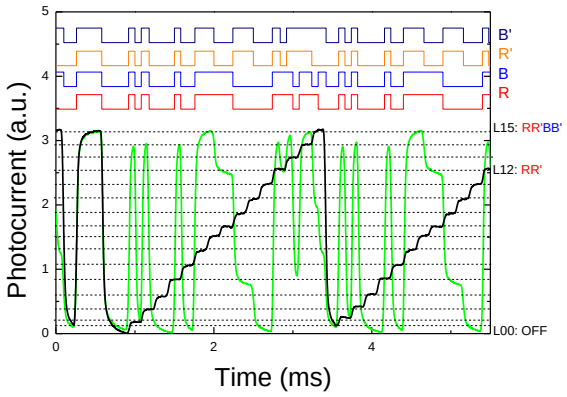

Figure 12. Photocurrent signal acquired along the forward path at cell central position under the coverage of RR'BB'.

The comparison of the output signal with the calibration curve allows the decode of the signal and identification of the receiver's position. Bit decoding of the multiplexed signal resulted for the CELL ID block the word 001010000100 (every 4 transmitters), corresponding to line 5 and column 2, for the POSITION block to the word 111111000000 from R and B transmitters and word 111000111000 from R' and B' transmitters, which indicates that the vehicle is at the center of the navigation cell. For the RACK block it is decoded the words 1110 from R and B transmitters and 1011 from R' and B' transmitters, which means that all racks of the cell are available with exception to the second rack in forward direction.

In Figure 13a) it is displayed the error control signal obtained with parity check bits of the transmitted signal of the I2V link shown in Figure 12.

The use of the calibration curve for decoding the multiplexed signal, demands a periodic transmission of the 16 possible combinations of the 4 optical signals to provide update of the calibration data and ensure correct output signal assignment. In this application, speed is not a critical issue, and this procedure does not overload the transmission efficiency. However, it can be discarded or done with less frequency when the accuracy of the decoding is increased using parity check bits.

The system is also feasible to be enhanced using feedback control for adjustment of the LED driving currents when the output photocurrent levels generated by the photodiode become too close. This procedure would minimize decoding errors due to parasitic effects such as optical intensity variations caused by to multiple reflections, light dispersion, or other light sources. Thus, the ambient light would not affect the proposed methodology.

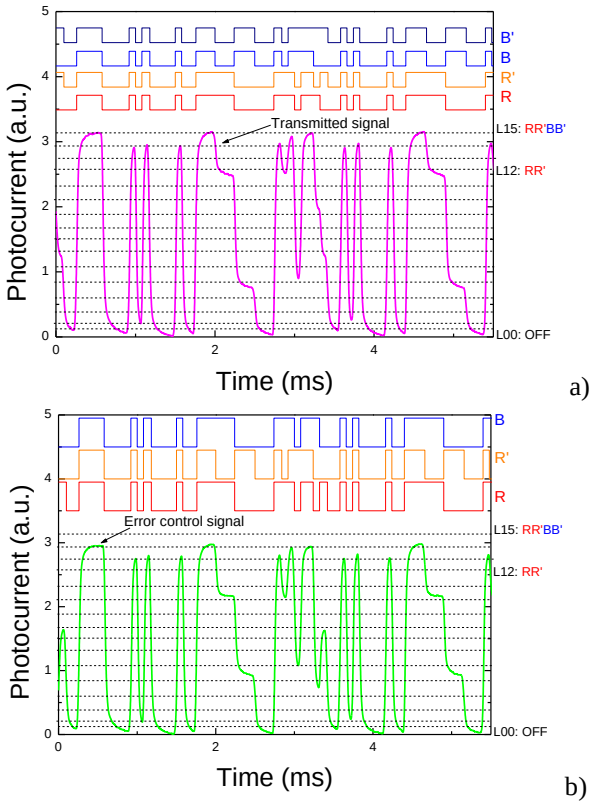

Figure 13. a) Transmitted signal by the I2V link and b) correspondent error control signal.

In addition to this bit error control strategy that improves the communication robustness, other coding schemes can be implemented, such as Manchester. OOK is a valuable modulation scheme in VLC due to its low complexity and ease of implementation. However, it may include flickering effects, which disturb the illumination distribution and even the communication under low dimming conditions.

The use of Manchester codes demands the use of two bits to transmit each symbol, which halves the data rate. However, it is prone to cause less hysteresis effects ensuring a stable calibration curve in better agreement with the level of each optical excitation.

IV. CONCLUSIONS

Bi-directional communication using VLC in both downlink and uplink channels has been addressed in a autonomous vehicle guidance system. The proposed indoor application deals with infrastructure to vehicle (I2V) and vehicle to infrastructure (V2I) communication in a warehouse. The vehicle moves autonomously through the warehouse transporting goods from the carts to the packaging station. The transmitted data is encoded in a 64 bits word, defined using specific data frames in communication channel. Codification of the optical signals ensured synchronization between frames. The code word of each channel was designed to ensure synchronization between

frames, to transmit information of the transmitter identification and of spatial location. Experimental evaluation demonstrated that the decoding solution can provide robust communications, especially if automatic bit error control is implemented in the optical domain. The optical sources using trichromatic LEDs were fully characterized by the Lambertian model adapted to the specifications of each LED. This provided the definition of footprint maps, necessary to enhance the accuracy of the position inside each navigation cell.

In addition, to the mentioned above relating the decoding process, other coding schemes may be implemented in future developments of the proposed system, namely Manchester codes.

ACKNOWLEDGEMENTS

This work was sponsored by FCT – Fundação para a Ciência e a Tecnologia, within the Research Unit CTS – Center of Technology and systems, reference UID/EEA/00066/2020 and IPL/2022/POSEIDON_ISEL.

REFERENCES

[1] P. Louro, M. Vieira, M. A. Vieira, "VLC Footprint Maps for Positioning and Guidance", ALLSENSORS 2022: The Seventh International Conference on Advances in Sensors, Actuators, Metering and Sensing, June 26-30, Porto, Portugal. ISBN: 978-1-61208-987-4, pp. 25-29.

[2] R. Mautz, "Overview of Current Indoor Positioning Systems", Geodesy Cartogr., vol. 35, pp. 18–22, 2009.

[3] Y. Gu, A. Lo, and I. Niemegeers, "A Survey of Indoor Positioning Systems for Wireless Personal Networks," IEEE Commun. Surv. Tutor., vol. 11, pp. 13–32, 2009.

[4] A. M. Căilean and M. Dimian, "Current Challenges for Visible Light Communications Usage in Vehicle Applications: A Survey", IEEE Communications Surveys & Tutorials, vol. 19, no. 4, pp. 2681-2703, 2017.

[5] M. Z. Chowdhury, M. T. Hossan, A. Islam, and Y. M Jang, "A Comparative Survey of Optical Wireless Technologies: Architectures and Applications", IEEE Access, vol. 6, pp. 9819-9840, 2018.

[6] G. Cossu, A. M. Khalid, P. Choudhury, R. Corsini, and E. Ciaramella, "3.4 Gbit/s Visible Optical Wireless Transmission Based on RGB LED," Optics Express, vol. 20, pp. B501–B506, 2012.

[7] M. Kavehrad, "Sustainable Energy-Efficient Wireless Applications Using Light", IEEE Communications Magazine, vol. 48, no. 12, pp. 66-73, 2010.

[8] E. F. Schubert and J. K. Kim, "Solid-state light sources getting smart", Science, vol. 308, no. 5726, pp. 1274-1278, 2005.

[9] J.-Y. Sung, C.-W. Chow, and C.-H Yeh, "Is blue optical filters necessary in high speed phosphor-based white light LED visible light communications?", Optics Express, vol. 22, no. 17, pp. 20646-20651, 2014.

[10] H. Le Minh et al., "High-speed visible light communications using multiple-resonant equalization," IEEE Photon. Technol. Lett., vol. 20, no. 14, pp. 1243–1245, 2008.

[11] A. M. Khalid, G. Cossu, R. Corsini, P. Choudhury, and E. Ciaramella, "1-Gb/s transmission over a phosphorescent white LED by using rate-adaptive discrete multitone modulation", IEEE Photon. J., vol. 4, no. 5, pp. 1465–1473, 2012.

[12] Z. Zhou, M. Kavehrad, and P. Deng, "Energy efficient lighting and communications", Proc. SPIE 8282, Broadband Access Communication Technologies VI, vol. 8282, pp. 82820J-1-82820J-15, 2012.

[13] A. Jovicic, J. Li, and T. Richardson, "Visible Light Communication: Opportunities, Challenges and the Path to Market", IEEE Communications Magazine, vol. 51, no. 12, pp. 26-32, 2013.

[14] P. Louro et al., "Optical demultiplexer based on an a-SiC:H voltage controlled device", Phys. Status Solidi C, vol. 7, no. 3–4, pp. 1188–1191, 2010.

[15] P Louro, V Silva, I Rodrigues, M.A. Vieira, M Vieira "Transmission of Signals Using White LEDs for VLC Applications" - Materials Today: Proceedings, 3(3), 2016, pp. 780–787 doi:10.1016/j.matpr.2016.02.009.

[16] M. Vieira, M. A. Vieira, P. Louro, V. Silva, and P. Vieira, "Optical signal processing for indoor positioning using a-SiC:H technology", Opt. Eng., vol 55, no. 10, pp. 107105-1-107105-6, 2016.

[17] M. A. Vieira, M. Vieira, P. Louro, and P. Vieira, "Cooperative vehicular communication systems based on visible light communication," Opt. Eng., vol. 57, no. 7, pp. 076101, 2018.

[18] P. Louro, V. Silva, M. A. Vieira, and M. Vieira, "Viability of the use of an a-SiC:H multilayer device in a domestic VLC application", Phys. Status Solidi C, vol, 11, no. 11–12, pp. 1703–1706, 2014.

[19] P. Louro, J. Costa, M. Vieira, M. A. Vieira, and Y. Vygranenko, "Use of VLC for indoor navigation with RGB LEDs and a-SiC:H photodetector", Proc. of SPIE, Optical sensors, vol. 10231, pp. 102310F-1-102310F-10, 2017.

[20] P. Louro, J. Costa, M. A. Vieira, and M. Vieira, "Optical Communication Applications based on white LEDs", J. Luminescence, vol. 191, pp. 122-125, 2017.

[21] M. Vieira, M. A. Vieira, I. Rodrigues, V. Silva, and P. Louro, "Photonic Amorphous Pi'n/pin SiC Optical Filter Under Controlled Near UV Irradiation", Sensors & Transducers, vol. 184, no. 1, pp. 123-129, 2015.

[22] Y. Qiu, H.-H. Chen and W.-X. Meng, "Channel modeling for visible light communications—a survey", Wirel. Commun. Mob. Comput. 2016; 16:2016–2034, DOI: 10.1002/wcm.

[23] I. Raza, S. Jabeen, S. R. Chaudhry, S. Asad Hussain, "Optical Wireless Channel Characterization For Indoor Visible Light Communications", Indian Journal of Science and Technology, Vol 8 (22), DOI: 10.17485/ijst/2015/v8i22/70605, 2015.

[24] P. Louro, M. Vieira, M. A. Vieira, "Bidirectional visible light communication," Opt. Eng. 59(12), 127109 (2020), doi: 10.1117/1.OE.59.12.127109.

[25] P. Louro, M. Vieira, and M. A. Vieira "Indoor and outdoor geo-localization and navigation by visible light communication", Proc. SPIE 11713, Next-Generation Optical Communication: Components, Sub-Systems, and Systems X, 117130H (5 March 2021); https://doi.org/10.1117/12.2579342.

[26] M. A. Vieira, M. Vieira, P. Louro, L. Mateus, P. Vieira, "Indoor positioning system using a WDM device based on a-SiC: H technology", Journal of Luminescence 191, pp. 135-138.

[27] P. Louro, M. Vieira, M. A. Vieira, M. Fernandes and J. Costa (2011), "Use of a-SiC:H Photodiodes in Optical Communications Applications", Advances in Photodiodes, Gian Franco Dalla Betta (Ed.), ISBN: 978-953-307-163-3, InTech, Chap.19, pp:377-402 (2011).

[28] Datasheet with technical specifications: https://media.digikey.com/pdf/Data%20Sheets/CREE%20Power/CLV1A-FKB_Rev5.pdf, March 2020.

[29] Y. Zhu, W. Liang, J. Zhang, and Y. Zhang, "Space-Collaborative Constellation Designs for MIMO Indoor Visible Light Communications", IEEE Photonics Technology Letters, vol. 27, no. 15, pp. 1667–1670, 2015.

[30] S. I. Raza, et al., "Optical Wireless Channel Characterization For Indoor Visible Light Communications", Indian Journal of Science and Technology, vol. 8, no. 22, pp. 1 – 9, 2015.

[31] M.V. Bhalerao, M. Sumathi, and S.S. Sonavane, "Line of sight model for visible light communication using Lambertian radiation pattern of LED", International Journal of Communication Systems, 2016, https://doi.org/10.1002/dac.3250.

[32] M. A. Vieira, M. Vieira, P. Louro, V. Silva, A. S. Garção, "Photodetector with integrated optical thin film filters", Journal of Physics: Conference Series 421 (1), 012011.